Received: 11 May 2020 | Revised: 23 December 2020 | Accepted: 7 February 2021

DOI: 10.1002/2050-7038.12869

RESEARCH ARTICLE

WILEY

Design of a high power density Halbach BLDC motor for an electric vehicle propulsion

B. V. Ravikumar[1,2] | **K. Sivakumar**[1] | **S. Karunanidhi**[2]

[1]Department of Electrical Engineering, Indian Institute of Technology Hyderabad (IITH), Hyderabad, India

[2]Control System Laboratory, RCI, Hyderabad, India

Correspondence
B. V. Ravikumar and K. Sivakumar, Department of Electrical Engineering, Indian Institute of Technology Hyderabad (IITH), Hyderabad, India.
Email: ee14resch01007@iith.ac.in (B. V. R.) and ksiva@iith.ac.in (K. S.)

Summary

The electric drives used for vehicle propulsion need to be highly efficient and high power dense to improve the performance of electric vehicles (EV) and make them competent in transportation applications. In the similar lines, this paper proposes a radial flux brushless direct current (BLDC) motor with surface magnet rotor with a Halbach array. The magnetic equivalent circuit of the motor is derived; nonlinear electromagnetic analysis carried out and arrived at performance characteristics for an EV propulsion. The proposed topology is compared with conventional BLDC motor with surface mount magnets and found an increment of 20% in power density. The hardware is realized, tested for its performance and the results are closely matching with design parameters.

KEYWORDS

electric vehicle, power density, BLDC motor, Halbach array

1 | INTRODUCTION

Improved power density topologies for electric drives are need of the day, which will lead to energy efficient drives for critical applications. Electric vehicle (EV) propulsion is one of the such application where high power density drives are required. BLDC motors are commonly used as drive in EV propulsion applications due to their high power density and efficiency.[1] In BLDC family, axial flux BLDC with dual stator and dual rotor structure is capable of producing high torque densities .[2-5] However, the disadvantage of axial flux topology is the necessity of manufacturing the laminations circumferentially and hence soft magnetic composites have to be used; whereas, the manufacturing of radial flux topology is well-established and magnetic materials of superior properties can be used. In the similar lines high power density topologies in radial flux family has been the point of focus to the researchers and lead to development of dual rotor structure capable of producing high power density.[6,7] The cost factor is major element in dual rotor structure, which will be increased due to usage of two bearings and corresponding stator housing fabrication and if we are looking for high power density with cost-effective solution, probably dual rotor structure will not suffice.

All the above literature used the rotor as surface magnet mount rotor to arrive at maximum flux density from permanent magnets (PMs). Halbach array magnets can improve the power density with surface magnet motor, the same is presented as design and analysis of enclosed rotor Halbach array BLDC motor.[8] The concept of Halbach array magnet

List of Abbreviations: $Ø_g$, air gap flux; $Ø_r$, remnant flux of main magnet; Pm, Magnet internal permeance; Rm, reluctance of magnet; $Ø_b$, Remnant flux of auxiliary magnet; P_b, Permeance of auxiliary magnet; R_b, reluctance of auxiliary magnet; R_s, Stator core reluctance; R_r, Rotor Core reluctance; R_g, Air gap reluctance; $Ø_g^1$, Halbach magnet flux; $Ø_g^2$, Rotor core flux; H, Field Intensity of main magnet; B, flux density of main magnet; J, current density; E, electric field; V, Volume enclosing; H_b, Field Intensity of main magnet; B_b, flux density of main magnet; W_m, Remanent flux density; B_r, Stored magnetic energy; A_r, Magnetic vector potential; EV, Electric Vehicle; BLDC, BrushLess DC; PM, Permanent Magnet; HB-BLDC, Halbach-BrushLess DC; FE, Finite Element; L-HMA, Linear-Halbach Magnetic Array.

maximizes the flux density in one direction and it was first presented by Mallinson as a magnetic curiosity.[9] Analysis of flux concentration effect carried out on ironless Halbach BLDC motor to improve the overall power density.[10] Different topologies of Halbach BLDC motor are analyzed and compared for high power density applications.[11] Further, it is shown that introduction of Halbach array to a dual PM rotor enhanced the power density by 38%, which could be good solution for vehicle propulsion.[11]

Not all the above literature with Halbach topology includes the detailed equations, sizing of Halbach magnets and magnetic circuit for solving magnetic parameters. This paper presents the design of Halbach BLDC motor in detail with complete design flowchart, magnetic design, nonlinear electromagnetic analysis and performance analysis, and compared with conventional surface mount magnet BLDC motor.

2 | PROPOSED HALBACH BLDC MOTOR

Figures 1 and 2 show the complete construction of Halbach BLDC motor (HB-BLDC). The stator carries the winding and is the stationary part. Rotor is mounted with main magnets and auxiliary magnets to form Halbach array. The design specifications are given in Table 1.

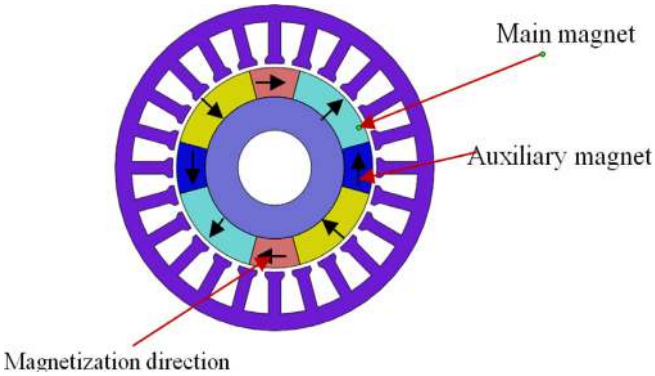

FIGURE 1 2D view of Stator and Rotor of HB_BLDC

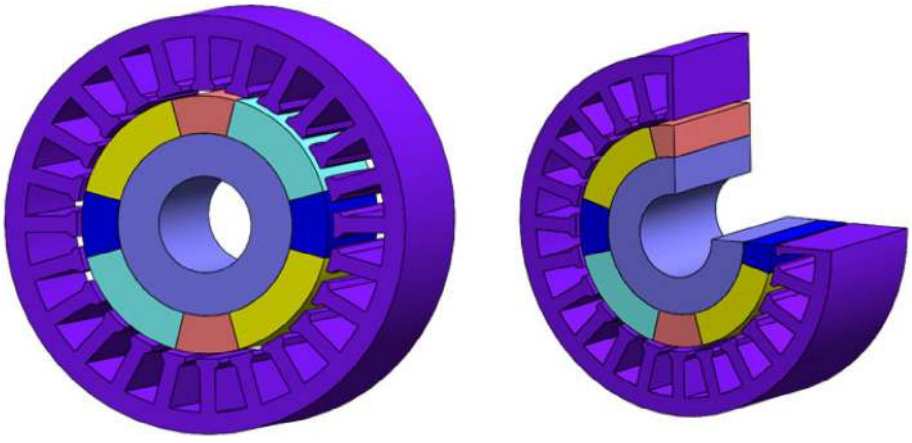

FIGURE 2 3D view of complete HB_BLDC motor assembly

TABLE 1 Specifications of HB_BLDC

S. no	Parameter	Value
1	Rated speed	2000 rpm
2	Rated torque	4.0 N m
3	Rated current	19 A
4	Rated voltage	48 V

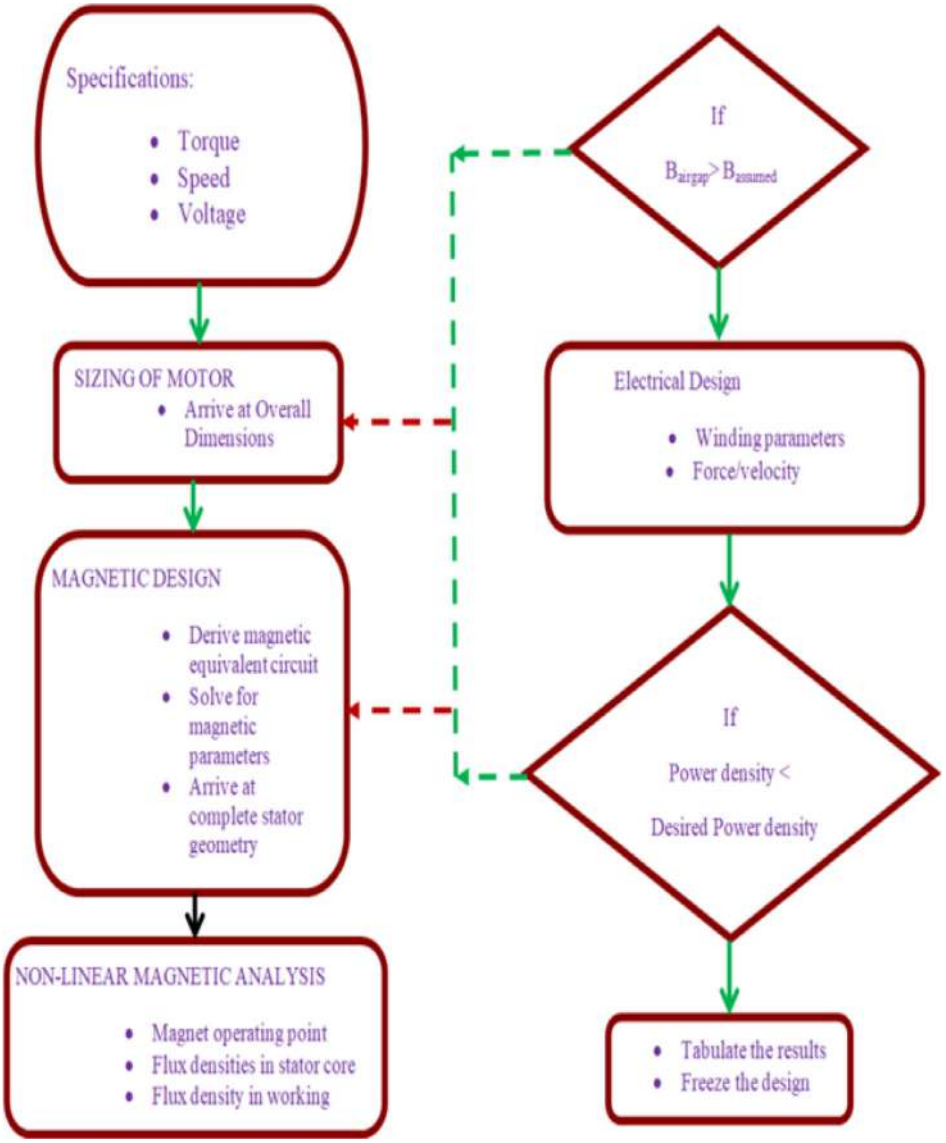

FIGURE 3 Design flowchart of Halbach-BLDC motor

3 | DESIGN OF HB-BLDC MOTOR

Based on the input specifications, the design of the motor is carried out. The complete design flow chart of the motor is given in Figure 3. The decisive parameters in the design are max.flux density allowable in stator core (taken as 1.5 T as the core material is steel) and the desired power density of the motor.

3.1 | Concept of Halbach array

The concept of Halbach array can be explained from Figure 4. As shown in Figure 4, the auxiliary magnets arranged in such an orientation to cancel main magnet flux on one side and add to the main flux on the other side. The same is illustrated in Figure 5 with finite element analysis carried out on planar model with main magnet and Halbach magnets.

From Figure 5, it can be observed due to the introduction of auxiliary magnets in specific orientation, the flux on the top side increased and almost negligible on the bottom side.

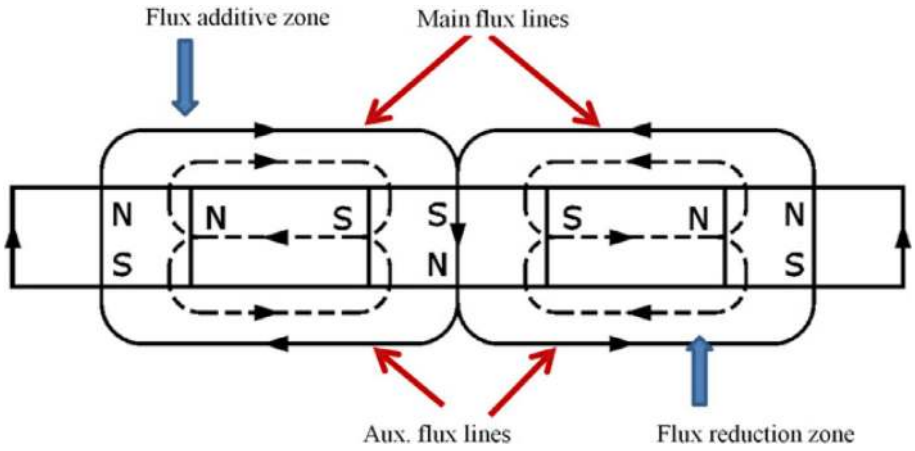

FIGURE 4 main Flux and auxiliary flux paths in Halbach arrangement

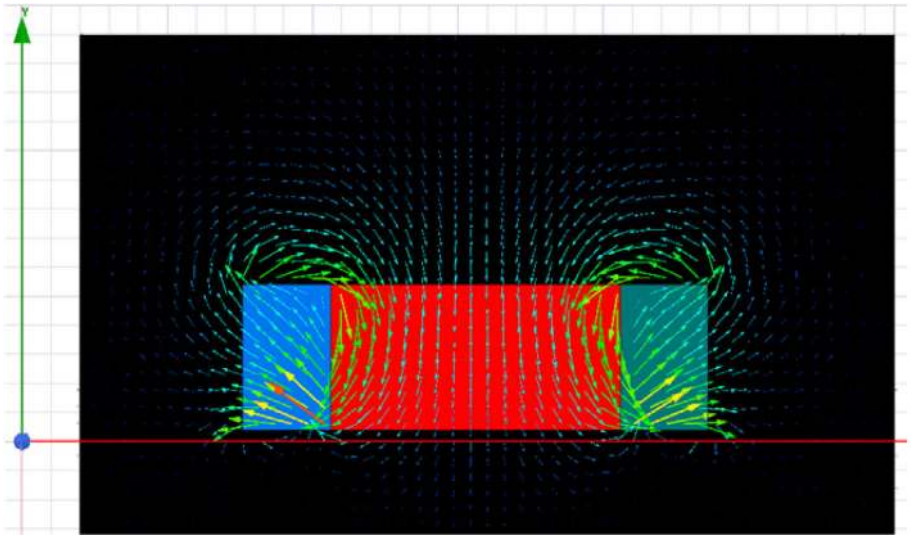

FIGURE 5 illustration of one-sided flux with Halbach-array using finite-element analysis

3.2 | Magnetic equivalent circuit

The magnetic equivalent circuit of the Halbach-motor is derived and solved for magnetic parameters. The main magnets and Halbach magnets are modeled as current sources. The reluctance of core is neglected as it is very less compared to air gap reluctance. The equivalent circuit is shown in Figure 6.

The following are the parameters used in the circuit followed by derived equations from the magnetic equivalent circuit:

- Øg = air gap flux.
- Ør = remnant flux of main magnet
- Pm = magnet internal permeance.
- Rm = reluctance of magnet.
- Øb = remnant flux of auxiliary magnet.
- Pb = permeance of auxiliary magnet.
- Rb = reluctance of auxiliary magnet.
- Rs = stator core reluctance.
- Rr = rotor core reluctance.
- Rg = air gap reluctance.
- φ_g^1 = Halbach magnet flux
- φ_g^2 = rotor core flux

FIGURE 6 Magnetic equivalent circuit of Halbach BLDC motor

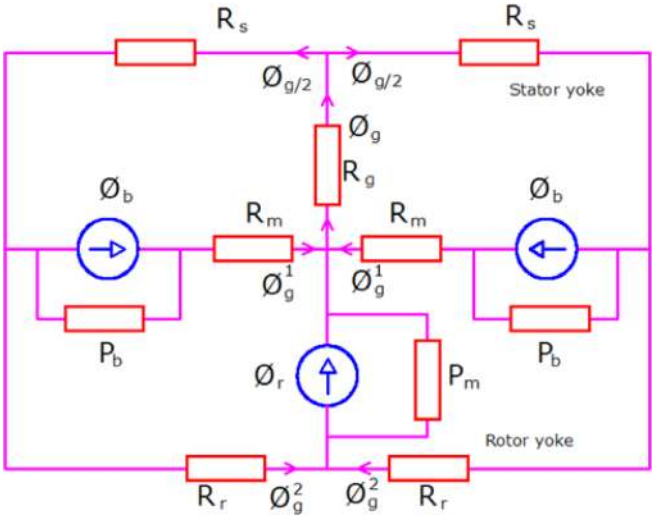

TABLE 2 Magnetic parameters in the machine at no load

S. no	Parameter	Value
1	Air gap reluctance	1.665e6AT/Wb
2	Main magnet permeance	1.133e-7wb/AT
3	Air gap flux density	0.95 T

Solving the magnetic equivalent circuit gives Equations (1)–(4), as shown below:

$$\varphi_g + \frac{\varphi_g R_g R_s - 2\varphi_b R_b}{R_m + R_b} + \frac{\varphi_g R_g R_s - 2\varphi_r R_m}{2R_m + R_r} = 0 \tag{1}$$

Since Rs <<<< Rm; Rs <<<< Rb, we are neglecting Rs and Rr

$$\varphi_g + \frac{2\varphi_g R_g - 2\varphi_b R_b}{R_m + R_b} + \frac{\varphi_g R_g - \varphi_r R_m}{R_m} = 0 \tag{2}$$

$$\varphi_g (R_m + R_b) R_m + \left(2\varphi_g R_g - 2\varphi_b R_b\right) R_m + \left(\varphi_g R_g - \varphi_r R_m\right)(R_m + R_b) = 0. \tag{3}$$

$$\varphi_g = \frac{2\varphi_b R_m + \varphi_r R_m + \frac{\varphi_r R_m^2}{R_b}}{R_m + R_g + \frac{R_m^2}{R_b} + \frac{3R_g R_m}{R_b}} \tag{4}$$

Above equations are solved to arrive at important magnetic parameters of the motor and finalize the complete geometry of the machine. Important magnetic parameters are tabulated in Table 2.

3.3 | Mathematical analysis: sizing of auxiliary magnet

The Halbach array increases the flux density on one side and reduces the flux density on the other side of the magnets. This can be utilized to increase the air gap flux density and thus the torque and power capability of the machine can be enhanced.

The dimensions of the auxiliary magnet plays major role in the increment of air gap flux density and effects the overall power density of the machine. Figure 7 shows the variation of air gap flux with variation in reluctance and area of auxiliary magnets.

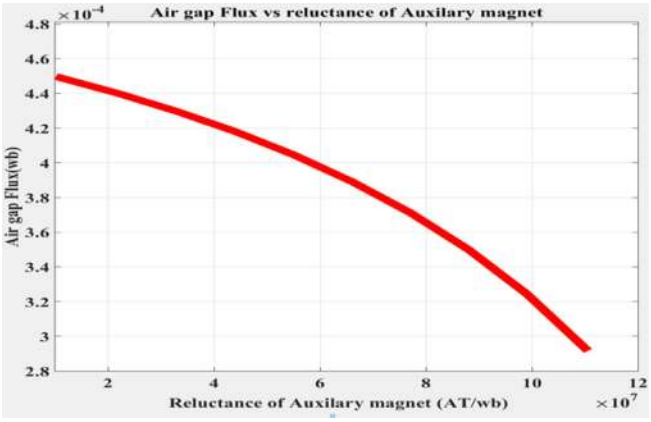

FIGURE 7 Air gap flux vs reluctance of auxilary magnet

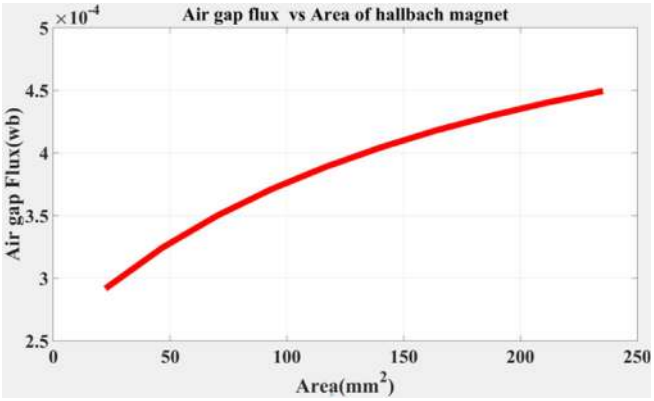

FIGURE 8 Air gap flux vs area of Halbach magnet

As shown in Figure 8, the air gap flux is increasing with increase in auxiliary magnet area and reduces as reluctance of auxiliary magnet is increasing. The design can be optimized to increase the area and reduce the internal reluctance of auxiliary magnets to maximize the flux density and hence the power density of the machine.

3.4 | Nonlinear magnetic analysis (finite element analysis)

The magnetic material characteristics are nonlinear in nature and have to be taken care in arriving at magnetic parameters of the motor. Finite element analysis is carried out on the motor by taking the nonlinear B-H characteristics of the material into account. The magnetic material used in the analysis is Cobalt-iron alloy, vacoflux-48, and the characteristics of the same are shown in Figure 9. The PMs used are NdFeB grade: 40 for both main and auxiliary magnets. The following formulation and boundary conditions are used in the finite element analysis to arrive at complete simulation of the machine.

3.4.1 | Finite element formulation

The FE analysis is carried out to maximize the magnetic vector potential of all elements in the FE model. The boundary condition of the model is maximizing the energy functional, which is achieved by setting magnetic vector potential A to zero at the outer periphery elements of stator. The following equations apply.

The finite element method is based on the energy conservation and for electric machine it is given as follows:

$$-\int_v \bar{E}.\bar{J}dV = \frac{\partial}{\partial t}\int_v \left(\int_0^B \bar{H}.d\bar{B} + \int_0^{Bb} \bar{H}_b.d\bar{B}_b\right)dV$$

The term on the right hand side is the rate of increase of the stored magnetic energy.

FIGURE 9 Magnetic material characteristics

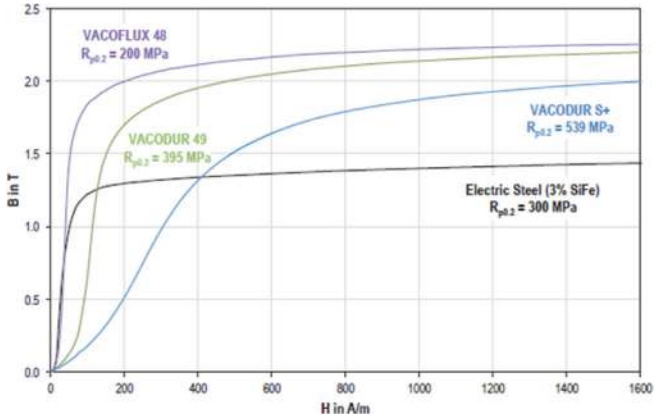

TABLE 3 Magnetic parameters at no load (FE analysis)

S. no	Parameter	Value
1	Avg. air gap flux density	1.0 T
2	Max. flux density in stator core	1.9 T
3	Max. flux density in mover core	1.35 T

$$W_m = \int_v \left(\int_0^B \bar{H}.d\bar{B} + \int_0^{Bb} \bar{H}_b.d\bar{B}_b \right) dV$$

The input power P_E may be expressed in terms of magnetic vector potential $\bar{A}$ rather than by $\bar{E}$ using the definition of $\bar{A}$.

$$\bar{B}_r = \bar{\nabla} \times \bar{A}_r$$

$$\bar{\nabla} \times \bar{E} = -\frac{\partial \bar{B}}{\partial t}$$

where $\bar{H}$ is the field Intensity of main magnet; $\bar{B}$ is the flux density of main magnet; $\bar{J}$ is the current density; $\bar{E}$ is the electric field; V is the volume enclosing; $\bar{H}_b$ is the field Intensity of main magnet; and $\bar{B}_b$ is the flux density of main magnet.

The magnetic parameters of the machine are derived on no-load using the magnetic analysis using Ansys-Maxwell software and shown in Table 3. The flux density profile in the complete motor, stator core at no load is shown in Figure 10.

The air gap flux density distribution at no load for both Halbach and conventional configuration is shown in Figure 11, which is derived from FE results. From the plot, it can be observed that there is an increment of 20% in the average air gap flux density with proposed configuration; this in-turn improves the power delivered by the machine within same volume. The operating point of magnet in both configurations is shown in Figure 12, which shows that the proposed configuration improves the performance coefficient (PC) of the magnet in the circuit.

The improved performance of magnet in proposed configuration is due to Halbach magnets. This improves the permanence coefficient of the magnet which will be an added advantage in case of coreless design where the magnet thickness is not required to increase to improve the PC as it is inherently improved due to Halbach configuration.

3.5 | Load analysis-FE

Once the no-load magnetic design is completed to arrive at overall dimensions of the machine, the electrical design is carried out to arrive at important parameters of winding, current density, stator resistance and inductance. FE analysis is carried out to analyze the effect of armature reaction during peak load of the motor. The effect of armature reaction can be divided as cross-magnetisation and de-magnetisation. Cross magnetisation is affect occurring in normal

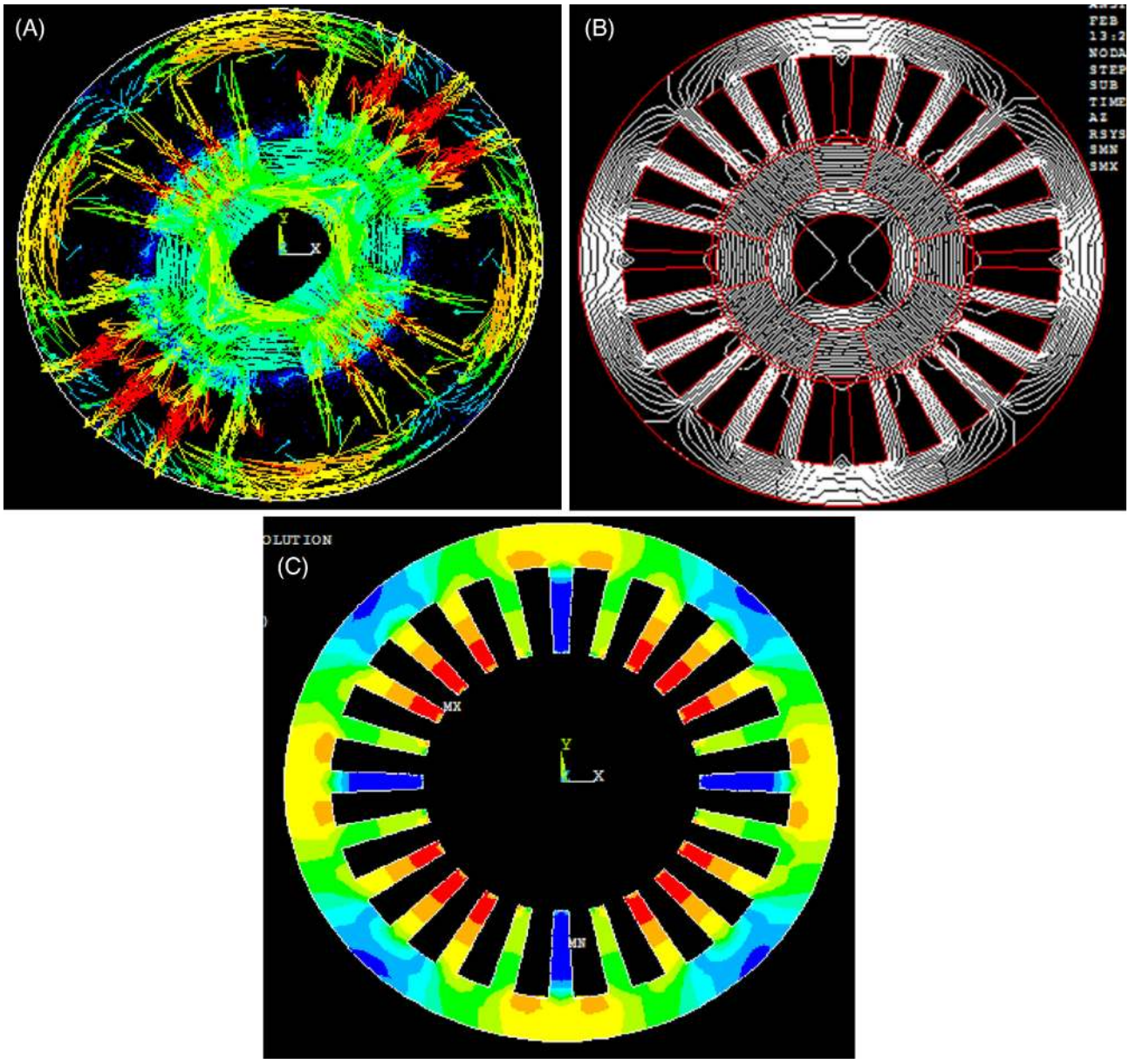

FIGURE 10 Vector plot of flux density and flux profile in actuator

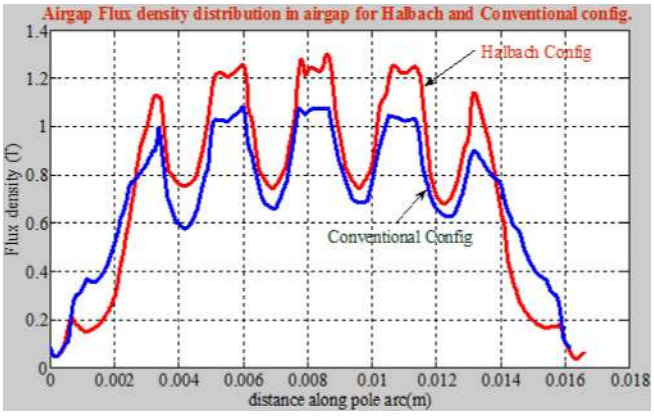

FIGURE 11 Air gap flux density distribution at no load (Halbach and conventional BLDC)

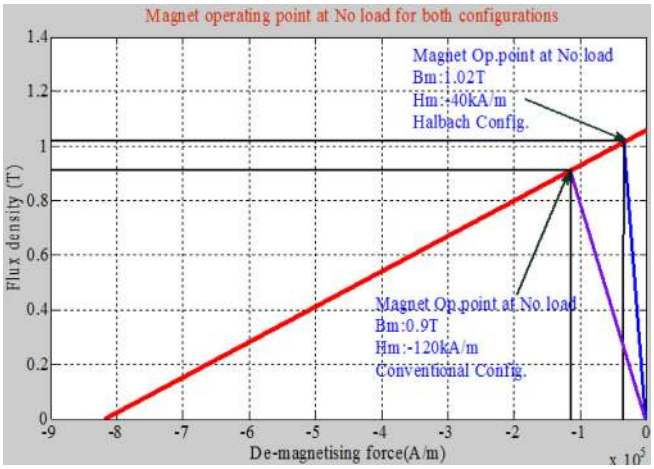

FIGURE 12 Magnet operating point at no-load for both configurations

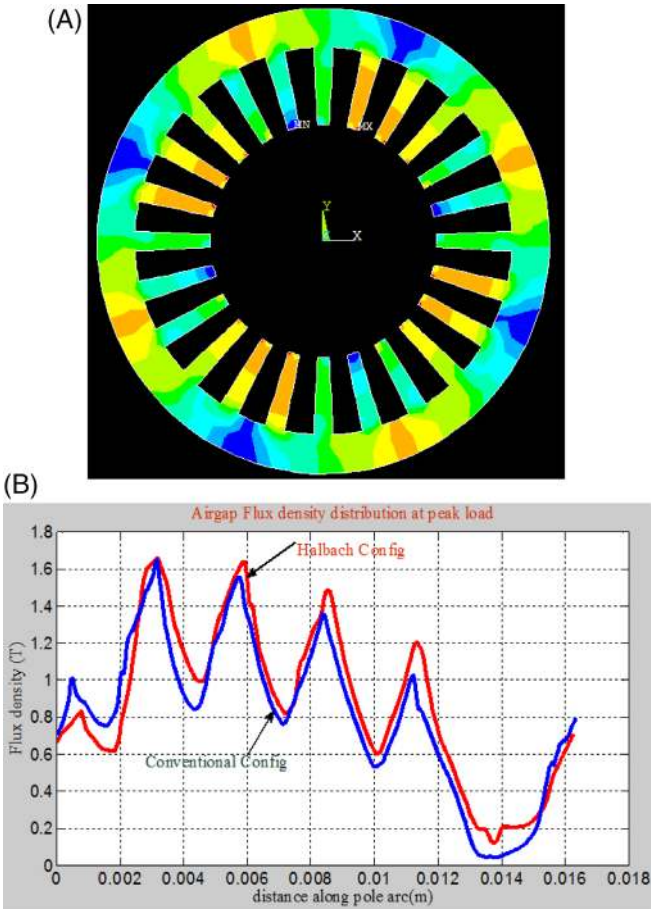

FIGURE 13 (A) Flux density in stator core at peak load. (B) Air gap flux density distribution at peak load

operating conditions, which distorts the air gap flux density distribution and gives rise to core losses. The average flux density distribution in stator core for peak loads is shown in Figure 13 along with air gap flux density curve. The max. Flux density in stator core is 2.25 T and rotor core is 1.9 T.

3.5.1 | Armature reaction: de-magnetization effect

De-magnetsation (de-mag) effect occurs during fault condition if the motor where the angle between d-axis and q-axis is 180°. This de-magnetizes the PM and shifts the operating point of the magnet down the de-magnetization curve. FE

Analysis has been carried out to analyze the performance of magnet under de-magnetsation. Airgap flux density during no load and peak load due to de-mag effect is shown in Figure 14 for both proposed and conventional configurations.

Due to De-mag effect the air gap flux density reduces and in turn shifts the operating point of magnet down the de-magnetization curve. The operating point of magnet in both configurations is shown Figure 15. The permeance coefficient in proposed configuration due to de-mag effect is 3.62, whereas in conventional configuration it is 2.0. This shows that the Halbach configuration is better in de-magnetization loads compared to conventional configuration of surface magnet mount rotors.

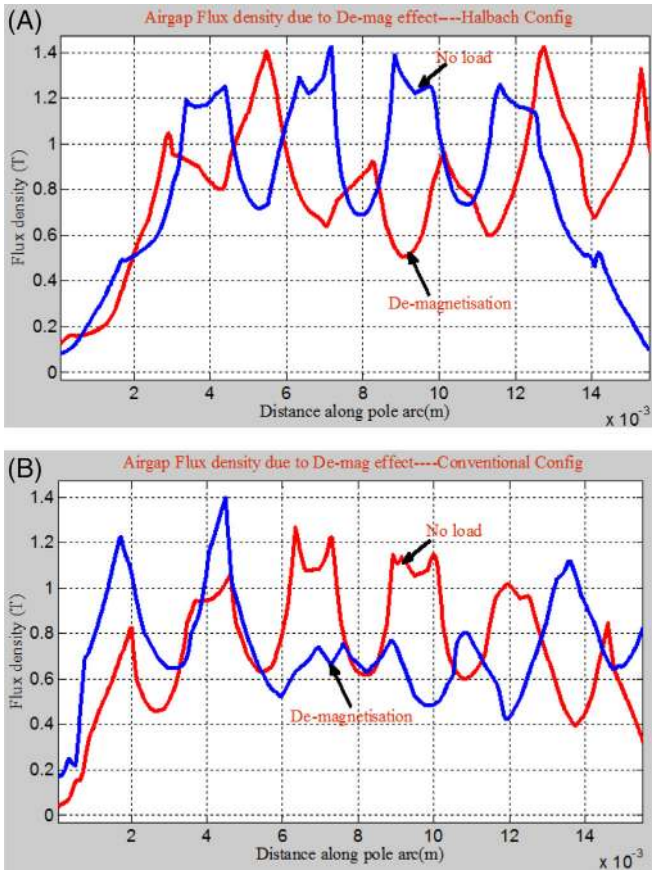

FIGURE 14 (A) Air gap flux density distribution De-mag effect-Halbach config. (B) Air gap flux density distribution De-mag effect-conventional config

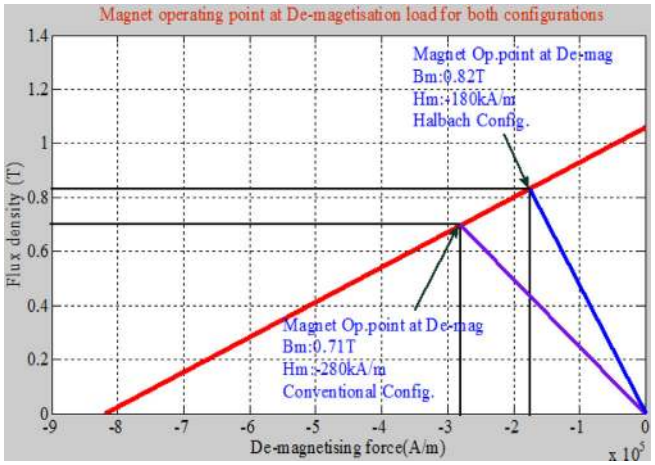

FIGURE 15 Magnet operating point due to De-mag load

3.6 | Current-torque characteristic of motor

The machine is loaded with peak current density corresponding to 19 A, that is, 40 A/mm^2 and FE analysis is carried out to arrive at current-torque characteristics of the motor and is shown in Figure 16. The characteristics of the both proposed and conventional configurations are compared and found that there is an increment of 20% in torque with the proposed Halbach BLDC motor, which improves the power by 20%.

4 | PROTOTYPE DVELOPMENT

The prototype of Halbach BLDC motor is realized and tested for its performance. The developed stator and rotor is shown in Figure 17. The rotor is fabricated with sleeve to protect the magnets from damage and retain them against the

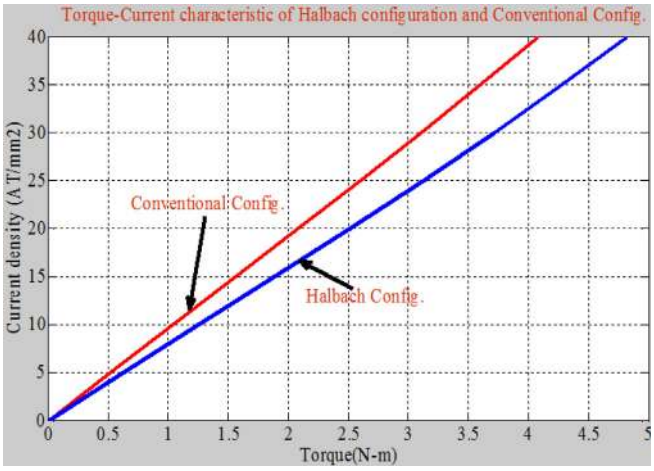

FIGURE 16 Torque-current characteristic of L-HMA and conventional linear magnetic actuator

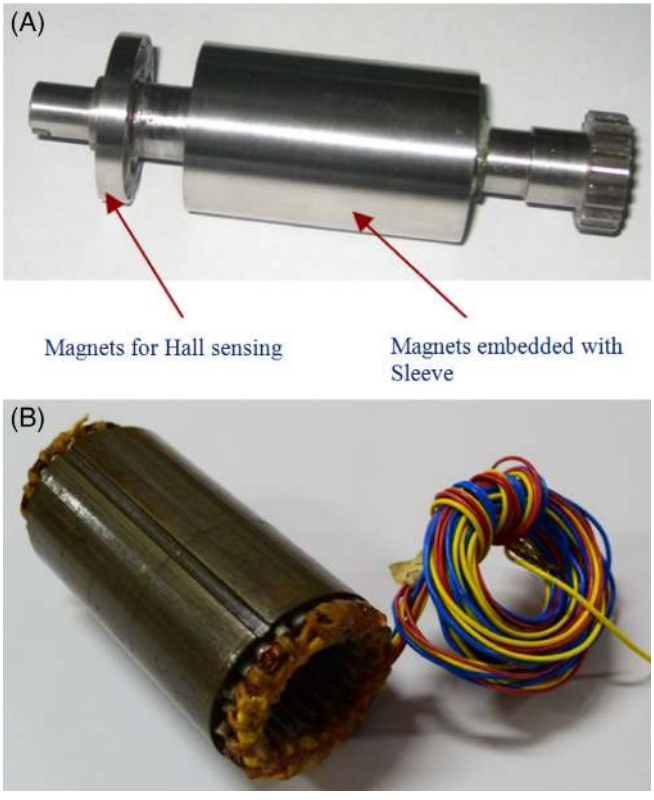

FIGURE 17 (A) Rotor of Halbach BLDC. (B) Stator of Halbach BLDC motor

FIGURE 18 Experimental set-up of Halbach BLDC motor

centrifugal force at higher speeds. The performance evaluation of motor is carried out to arrive at speed-torque, current-torque characteristics with help of dynamometer. The experimental set-up is shown in Figure 18.

5 | CONCLUSION

Halbach brushless DC motor is proposed for EV propulsion. Complete design of motor is given along with magnetic equivalent circuit, nonlinear electromagnetic analysis, and performance analysis of the machine. On load performance of the machine is analyzed by deriving the air gap flux density distribution and average flux density distribution in the core. Magnet operating point is derived and compared with conventional surface mount magnet rotor under no load and de-mag loads. Current-torque characteristics derived for both configurations and found an increment of 18% in torque with proposed Halbach configuration. Hardware is realized as per design and tested for performance with results matching fairly with design and simulated characteristics. The proposed Halbach BLDC motor definitely a viable solution for high power density applications.

PEER REVIEW

The peer review history for this article is available at https://publons.com/publon/10.1002/2050-7038.12869.

DATA AVAILABILITY STATEMENT

NIL

ORCID

K. Sivakumar https://orcid.org/0000-0002-4207-453X

REFERENCES

1. Zhu ZQ, Howe D. Electric machines and drives for electric, hybrid and fuel cell vehicles. *Proc IEEE*. 2007;95(4):746-765.
2. Qu R, Aydin M, Lipo TA. Performance comparison of dual-rotor radial-flux and axial-flux permanent-magnet BLDC machines. Paper presented at: Proceedings of the IEEE International Conference on Electrical Machines and Drives; Madison, WI; 2003. pp. 1948-1954.
3. Sitapati K, Krishnan R. Performance comparisons of radial and axial field permanent magnet brushless machines. *IEEE Trans Ind Appl*. 2001;37(5):1219-1226.
4. Simisie NB, Ertan HB. A comparison of torque capabilities of axial flux and radial flux type of brushless DC (BLDC) drives for wide speed range applications. Paper presented at: Proceedings of the IEEE PEDS; Honk Kong; 1999. pp.719-724.

5. Cavangninto A, Lazzari M, Profumo F, Tenconi A. A comparison between the axial flux and radial flux structures for PM synchronous motors. Paper presented at: IEEE IAS Annual Meeting, Vol. 3; Chicago, IL; 2001. pp. 1611-1618.
6. Qu R, Lipo TA. Dual-rotor, radial-flux, torodially wound, permanent-magnet machines. *IEEE Trans Ind Appl*. 2003;39(6):1665-1673.
7. Qu R, Lipo TA. Design and parameter effect analysis of dual-rotor radial flux, toroidally wound, permanent magnet machines. *IEEE Trans Ind Appl*. 2004;40(3):771-779.
8. Praveen RP, Ravichandran MH, Sadasivan Achari VT, Jagathy Raj VP, Madhu G, Bindu GR. Design and analysis of enclosed rotor Halbach array brushless DC motor for spacecraft applications. Paper presented at: XIX International Conference on Electrical Machines-ICEM 2010; 2010.
9. Mallinson JC. One-sided fluxes—a magnetic curiosity? *IEEE Trans Magn*. 1973;9(4):678–682.
10. Praveen RP, Ravichandran MH, Achari VTS, Jagathy VPR, Madhu G, Bindu GR. Design and analysis of zero cogging brushless dc motor for spacecraft applications. *ECTI Trans Electr Eng Electron Commun*. 2011;9(1):254–258.
11. Ravikumar BV, Sivakumar K. Design of a new dual rotor radial flux BLDC motor with Halbach array magnets for an electric vehicle. Paper presented at: IEEE International Conference on Power Electronics, Drives and Energy Systems (PEDES); 2016.

How to cite this article: Ravikumar BV, Sivakumar K, Karunanidhi S. Design of a high power density Halbach BLDC motor for an electric vehicle propulsion. *Int Trans Electr Energ Syst*. 2021;e12869. https://doi.org/10.1002/2050-7038.12869